Ab Initio Study of the Adsorption of NO on the Rh−6(+) Cluster

ARTICLE *in* THE JOURNAL OF PHYSICAL CHEMISTRY A · JUNE 2011

Impact Factor: 2.69 · DOI: 10.1021/jp202511w · Source: PubMed

4 AUTHORS:

M. Begoña Torres
Universidad de Burgos
30 PUBLICATIONS **268** CITATIONS
SEE PROFILE

F. Aguilera-Granja
Universidad Autónoma de San Luis Potosí
150 PUBLICATIONS **1,368** CITATIONS
SEE PROFILE

Carlos Balbás
Universidad de Valladolid
136 PUBLICATIONS **2,249** CITATIONS
SEE PROFILE

Andrés Vega
Universidad de Valladolid
175 PUBLICATIONS **1,950** CITATIONS
SEE PROFILE

THE JOURNAL OF PHYSICAL CHEMISTRY A

ARTICLE

pubs.acs.org/JPCA

Ab Initio Study of the Adsorption of NO on the Rh_6^+ Cluster

M. B. Torres,*[,†] F. Aguilera-Granja,[‡] L. C. Balbás,[§] and A. Vega[§]

[†]Departamento de Matemáticas y Computación, Universidad de Burgos, E-09006 Burgos, Spain

[‡]Instituto de Física, Universidad Autónoma de San Luis Potosí, 78000 San Luis Potosí, México

[§]Departamento de Física Teórica, Atómica y Óptica, Universidad de Valladolid, 47011 Valladolid, Spain

ABSTRACT: The process of NO adsorption on the cationic cluster Rh_6^+ is investigated using the density-functional theory (DFT) with the generalized gradient approximation (GGA) to exchange and correlation. We determine the geometries, electronic structure, and relevant energies for different structural and spin isomers of $Rh_6^{0,\pm}$, and we study the consecutive adsorption of two NO molecules on the cationic cluster Rh_6^+. With regard to the first NO molecule, different adsorption energies are found for the ground state octahedral structure of the bare cationic cluster and for the first isomer, which, having a prism-type structure, undergoes a structural transition to an octahedral symmetry upon dissociative adsorption of NO. Several dissociative NO adsorption processes are analyzed in comparison with molecular adsorption of NO to give support to the first step of the reaction inferred from experiments. With regard to the adsorption of a second NO molecule, the intermediate with lowest energy contains a preformed N_2 molecule. The energy of that complex is about 0.7 eV smaller than the sum of the free N_2 energy plus the lowest energy of the $Rh_6^+-O_2$ complex. This complex is composed of two separated O atoms occupying adjacent 2-fold bridging positions of the nearly undistorted Rh_6^+ octahedral cluster. These findings are in qualitative agreement with experiments.

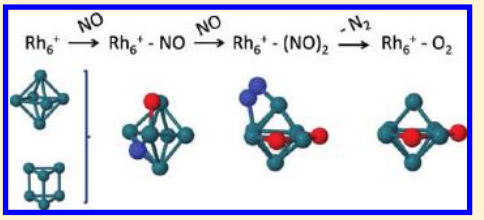

I. INTRODUCTION

Small metal clusters are nanostructures of great interest from both the fundamental and technological viewpoints. Their structural and electronic properties are different, in general, from those of the bulk and, furthermore, nonscalable for small enough sizes. This size regime, where one atom more (or less) makes the difference and quantum confinement effects are fundamental, houses a rich variety of geometrical structures, magnetic arrangements, optical properties, or catalytic properties that open new prospects in molecular electronics, spintronics, and catalysis and whose understanding is a challenge for the experimentalists and theoreticians in many branches of science like physics, chemistry, or medicine. The production of size selected free-standing clusters in cluster beams is well controlled at present. Free-standing rhodium clusters have been the matter of intense research as regards their magnetic,[1] electrical,[2] and catalytic properties.[3−8] Rhodium is known to be a good catalyst with applications, for instance, in automobile catalytic converters. In particular, rhodium is an active catalyst for CO oxidation and it is used, as well, in reducing nitrogen oxides NO_x.[9] The studies of rhodium surfaces in the context of catalytic reactions have shed light on the mechanisms of the CO and NO processes.[9−17] Small free-standing clusters, characterized by loss of coordination, structure relaxations that lead to particular symmetries, and a marked surface effect, are interesting forms of matter as regards the investigation of the catalytic properties in reducing nitrogen oxides NO_x. In the catalytic process to eliminate these pollutants, it is also important to avoid the undesirable partial reduction of NO to produce N_2O. Rhodium is a performant catalyst in this respect, due to its ability to adsorb and dissociate NO molecules without the subsequent formation of N_2O.

The reaction of nitric oxide on Rh_6^+ clusters has been investigated by Ford and co-workers through Fourier transform ion cyclotron resonance (FT-ICR) mass spectrometry.[4] More recently, Anderson et al. have extended these measurements to $Rh_n^{\pm}$ ($n < 30$) clusters.[5] Ford et al.[4] have found evidence for the formation of two different forms of the Rh_6^+, which react at very different rates with NO. Moreover, they propose a reaction mechanism based on the dissociative adsorption of NO on the surface of the cluster in the first reactions, producing the dioxides and tetraoxides and the rapid desorption of molecular nitrogen. To interpret the experimental data for the adsorption of more than one NO molecule, and on the basis of the observations of NO adsorption on the Rh(111) surface,[9,10,13,15] the authors proposed a reaction mechanism based on the dissociative adsorption of NO, and preferentially in 3-fold binding sites of an octahedral Rh_6^+. Later, Harding et al.[6] performed DFT calculations for the reaction of NO with two Rh_6^+ isomers, having square bipyramid structure and trigonal prism structure, respectively. They found three favorable reactions paths, two of them starting with the trigonal prism, and the third was associated with the square bipyramid structure. Thus, these authors provided support to interpret the observed biexponential reaction kinetics as an effect of structural isomerism.

Received: March 16, 2011
Revised: June 15, 2011
Published: June 21, 2011

However, the geometrical structures of free-standing clusters are difficult to characterize because most of the experimental techniques used in bulk-like systems are not suitable if the cluster is not supported on a host. And although it is possible to take advantage of the structural dependency of the adsorption of light molecules on the surface of the cluster,[18] the question arises whether the structure of the pure cluster is preserved upon adsorption. Other types of experiments, like trapped ion electron diffraction (TIED)[19] and infrared spectroscopy,[20] have shed light on the geometrical structure of metal clusters when combined with DFT total energy calculations. Recently, Hamilton and co-workers[21] have extended the infrared multiple photon dissociation spectroscopy (IR-MPD) into the far-infrared by the inert messenger technique combined with the intense radiation from a free-electron laser (FEL). In this way, more direct structural information on the metal framework is gained because the metal−metal modes can be probed directly. That technique has been applied to study the IR-MPD depletion spectra of $Rh_6N_2OAr_m^+$ complexes.[21] The results were rationalized by means of DFT calculations that predict an octahedral symmetry for the ground state of Rh_6^+ (with magnetic moment 9 μ_B) having the N_2O molecule chemisorbed on top of a Rh atom through an N−Rh bond (with binding energy 0.78 eV).[21] More recently, results of IR-MPD studies of $Rh_n-N_2O^+$ ($5 < n < 9$) complexes in both the mid-infrared and far-infrared regions have been reported.[22]

Therefore, to get a more complete picture of the adsorption processes of NO on the Rh_6^+ cluster, it is pertinent to perform a comprehensive theoretical study considering different scenarios for the NO adsorption on the most stable structural and spin isomers of the cationic cluster Rh_6^+, and by considering full structure optimization. We will give support to the experimental results, for the adsorption of the two first NO molecules on the Rh_6^+ cluster, and additionally, we will calculate the structural and energetic features of some intermediates. Thus, the aim of the present work is to seed further light on the understanding of the consecutive adsorption of NO molecules on the Rh_6^+ cation.

From the theoretical side, the coexistence of itinerant d-electrons with delocalized sp-electrons in the electronic valence of rhodium makes difficult its treatment within simple models. If the determination of both the geometry and electronic structure is being achieved at the same level, which is desirable due to the strong interdependence of both kinds of properties, DFT has been demonstrated to be a very efficient and reliable approach for a large variety of systems. Thus, Ghosh and co-workers[16] calculated recently, using DFT, the activation energies for NO dissociation on unstrained and strained Rh(100) surfaces and monolayers of Rh atoms on strained and unstrained MgO(100) surfaces. These authors were able to establish a new indicator of activation energies that collect both the chemical nature of the substrate and the strain imposed by the substrate. In other recent work, Rempel and co-workers[17] studied the dissociation path and thermochemistry of NO on flat, close-packed Rh(111) and stepped Rh(211) surfaces. They found that the presence of steps leads to an increase in the reaction exothermicity and to a decrease in the effective activation energy, so that NO dissociation at defect sites may dominate the process on close-packed Rh single crystal surfaces. Nevertheless, the studies on small metal clusters may not sufficiently recover the electronic structure of the surface[23] but have interesting features of their own.

The electronic structure, geometries, and magnetic properties of neutral Rh clusters have been investigated at the DFT level considering structural relaxations by different groups, including ours.[24−27] Interesting general trends were predicted, like, for instance, the magnetic character of small Rh clusters in contrast with the nonmagnetic character of their bulk counterpart. Details on the growth patterns and electronic properties have been discussed.

In our previous work on the free-standing neutral rhodium clusters, we used the SIESTA implementation (Spanish Initiative for Electronic Simulation of Thousands of Atoms)[28] of the DFT at the GGA level and we characterized, among others, the most stable structural and spin isomers of Rh_6. The same theoretical approach has been used here to extend this study first to the charged $Rh_6^{\pm}$ clusters. We have then studied the NO adsorption on both the ground state and the first isomer of Rh_6^+ in different ways (dissociatively or molecularly on top, bridge or hollow sites). We have calculated the relevant energies (total energy differences, adsorption energies). We have analyzed and discussed our results in the context of the experimental measurements of Ford et al.[4] and other available data.

The rest of the paper is organized as follows. In section II we briefly describe our DFT approach. In section III we present the results for the most stable structural and spin isomers of the neutral and charged $Rh_6^{0,\pm}$ clusters (subsection A), as well as for the NO adsorption on both the ground state and the first isomer of Rh_6^+ (subsection B) and the adsorption of a second NO molecule on low lying energy isomers of Rh_6^+−NO complexes (subsection C). In section IV we discuss the results. The main conclusions are summarized at the end.

II. THEORETICAL METHOD

We have performed our calculations using the DFT approach as implemented in the code SIESTA.[28] This method employs a linear combination of pseudoatomic orbitals as basis sets. The atomic core is replaced by a nonlocal norm-conserving Troullier−Martins[29] pseudopotential that is factorized in the Kleinman−Bilander form.[30] The code allows us to perform, together with the electronic calculation, structural optimization using a variety of algorithms. In the present study, we have used the GGA to the exchange and correlation potential as parametrized by Perdew, Burke, and Ernzerhof (PBE).[31] The ionic pseudopotentials were generated using the atomic configurations $4d^8$, $5s^1$, and $5p^0$ for Rh, $2s^2$ and $2p^3$ for N, and $2s^2$ and $2p^4$ for O. The s, p, and d cutoff radii were 2.18, 2.30, and 1.68 au for Rh, while the s and p cutoff radii for N (O) were both 1.24 (1.14) au. For Rh and N we have included nonlinear core corrections[32] to account for the significant overlap of the core charge with the valence orbitals and to avoid spikes that often appear close to the nucleus when the GGA approximation is used. We have verified that these pseudopotentials reproduce accurately the eigenvalues of different excited states of the respective isolated atoms.

Concerning the basis set and the energy cutoff to define the real space grid for numerical calculations involving the electron density, a detailed and careful test has been performed. We have described the valence states using double-zeta polarized (DZP) basis sets with two orbitals having different radial forms to describe both the 5s and the 4d shells and one orbital to describe the 5p shell of Rh and two orbitals having different radial forms to describe both the 2s and the 2p shells of N and O (the 2p with single polarized). We have considered a 250 Ry energy cutoff to define the real space grid for numerical calculations involving the electron density, and an electronic temperature of 25 meV to

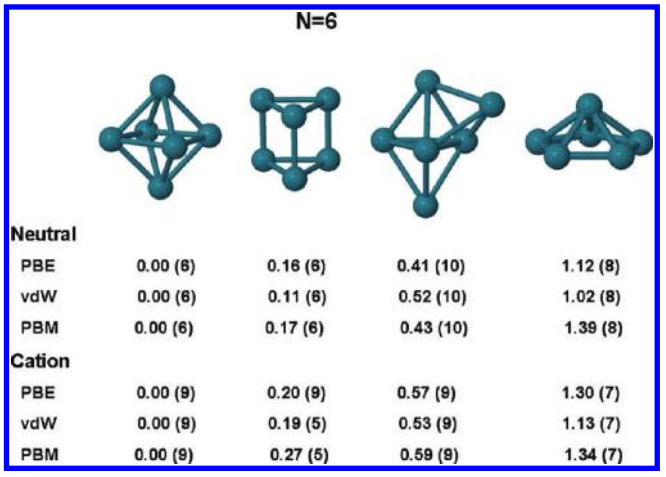

Figure 1. Low lying isomers of Rh_6 neutral and Rh_6^+ cationic clusters. The total energy difference with respect to the O_h ground state, in eV, and the magnetic moment, in μ_B (in parentheses), are given below for three different xc-functionals, PBE,[31] vdW,[37] and PBM[39].

accelerate the self-consistency. We have tested larger cutoffs and lower electronic temperatures for particular cases and they do not substantially modify the results. To optimize the geometrical structures, we have performed local relaxations using the conjugate gradient algorithm, starting from a large variety of initial structures having different symmetries and spin configurations (different structural and spin isomers).The structural optimization was stopped when each force component at each atom in the cluster was smaller than 6 meV/Å. For some particular clusters we have also used the fully unconstrained version of the SIESTA code to check the possible existence of noncollinear magnetic arrangements. We have found a collinear ferromagnetic-like order in all cases.

The adsorption energies in the Rh_6^+−NO systems are calculated by taking into account the counterpoise correction method[33] for removing the basis set superposition errors (BSSE). These errors arise due to the different dimension of the Hilbert spaces associated with the initial and final systems whose energy difference has to be computed. We have verified that using this procedure, the calculated binding energies of the dimers N_2, O_2, and NO are closer to the experimental values than without the BSSE correction, so that an improvement is also expected for the adsorption energies in the Rh_6^+−NO systems. Specifically, the binding energies of N_2, O_2, and NO with (without) BSSE correction are, in eV, 9.68 (10.39), 6.66 (6.71), and 7.34 (7.46), to be compared with the experimental values[34] 9.79, 5.16, and 6.53. Typical BSEE corrections for the NO adsorption energies reported in the Results section (Figure 3) are about 0.17 eV (0.20 eV) for dissociative (molecular) NO adsorption. Thus, BSSE correction improves the binding energy value of the different equilibrium compounds without changing substantially their relative energy.

III. RESULTS

A. Neutral and Charged $Rh_6^{0,\pm}$ Clusters. In our previous work on the free-standing neutral rhodium clusters,[27] we characterized, among others, the most stable structural and spin isomers of the neutral Rh_6 cluster. We have extended here the study to the cationic cluster Rh_6^+. For the sake of completeness,

Table 1. Total Energy Difference Relative to the Corresponding Lowest Energy State, Average Magnetic Moments per Atom, Average Distance, and Number of Total Bonds for the Different Isomers of Neutral and Charged Rh_6^ν Clusters ($\nu = 0, \pm 1$)

structure	ΔE (eV)	μ (μ_B/atom)	distances (Å)	total bonds
Neutral				
octahedron	0.00	1.00	2.59	12
triangular prism	0.16	1.00	2.50	9
capped triangular bipyramid	0.41	1.67	2.62	12
pentagonal pyramid	1.12	1.34	2.57	10
Positive Charge				
octahedron	0.00	1.50	2.64	12
triangular prism	0.20	1.50	2.50	9
capped triangular bipyramid	0.57	1.50	2.62	12
pentagonal pyramid	1.30	1.17	2.57	10
Negative Charge				
octahedron	0.15	1.83	2.62	12
triangular prism	0.00	1.17	2.50	9
capped triangular bipyramid	0.25	1.50	2.62	12
pentagonal pyramid	0.57	1.83	2.56	10

we have also calculated the anionic cluster Rh_6^-. We have considered a variety of structures as input. We have performed the calculations either by allowing the total spin to freely converge or by fixing the total spin of the cluster in various states different from the one resulting in the free calculation to ensure finding the ground state as well as the correct energetic order among the different spin and structural isomers.

In Figure 1 we show the four most stable structural isomers of Rh_6. For the sake of completeness we have optimized the electronic structure of Rh_6 and Rh_6^+ (starting with the PBE geometries shown in Figure 1) considering also two unconventional flavors of the GGA. The first is the van der Waals (vdW in the following) nonlocal energy functional of Dion et al.,[37] which have been recently implemented by Soler et al.[38] in the SIESTA code. The second is our implementation in SIESTA of a tightening of the Lieb−Oxford-bound on the PBE functional, recently discussed by Odashima et al.,[39] and that corresponds to the ratio $\lambda = \lambda_{EL} = 2$ in $E_{xc} \geq \lambda E_x^{LDA}$, which matches to the extreme low-density limit of the uniform electron liquid ($\lambda = \lambda_{LO} = 2.27$ in the standard PBE). We will refer to this xc-functional as PBM. We have used recently the PBE, vdW, and PBM functionals to optimize the structures "O_h+1" and "prism+1" of Rh_7 cluster,[27] with the result that "prism+1" with a magnetic moment of 9 μ_B is the lowest energy configuration for PBE and vdW functionals, but it is "O_h+1" for the PBM functional, with 10 meV higher binding energy per particle that the "prism+1" isomer. For the present $Rh_6^{0/+}$ calculations, we have obtained always the isomer O_h (actually a square bipyramid) as the lowest energy one within the three xc-functionals. The magnetic moment is 6 (9) μ_B for the neutral (cationic) species. Moreover, the relative energetic ordering order of the all low lying isomers of Rh_6 neutral and Rh_6^+ cationic clusters is the same for the three different

xc-functionals, PBE, vdW, and PBM. In this context, we note that some hybrid functional provides a better description of the potential energy landscape than the PBE one. For example, the hybrid PBE1 functional leads to Rh_8^+ geometry in good agreement with FIR-MPD spectrum.[40,41] On the other hand, both PBE and PBE1 functionals favor the same distorted octahedral structure for Rh_6^+, although the ordering of low lying energy isomers is found to be different. However, the PBE1 infrared spectra for Rh_6^+ is only relatively good for the octahedron case and less good for the two nearest low-energy isomers.[41] Thus, although hybrid functionals containing different amounts of exact exchange (25% in the PBE1 case) have been shown to be very efficient in the search of ground state and low lying energy isomers of certain clusters, we always prefer to use xc-functionals without empirical parameters fitting the binding energy of typical molecule sets.

Table 1 reports the differences in total energy (with respect to the most stable one), spin magnetic moments, and relevant structural properties for neutral and charged $Rh_6^{0,\pm}$, to compare the general trends. For neutral Rh_6, the difference in energy per atom between the octahedron (ground state) and the triangular prism (first isomer) is on the order of room temperature. The second and third isomers are, respectively, a capped triangular bipyramid and a pentagonal pyramid structures. The energetic order among the four structures of Rh_6^+ is the same as for Rh_6, with slightly larger energy differences between them. In addition, the loss of an electron is accompanied by a change of the spin state, not always in the same direction. The ground state and the prism isomers increase their total spin with respect to that of the neutral cluster, which correlates with a slight increase of the average interatomic distance, whereas the other two isomers in Table 1 decrease the total spin upon losing an electron while keeping the same average interatomic distance as their neutral counterparts (Table 1). Besides the correlation of spin magnetic moment and interatomic distances (the larger the interatomic distance, the higher is the spin magnetic in general due to electron localization), an increase of the interatomic distances is expected for the cationic clusters with respect to the neutral ones due to the reduced electron density in the cation, leading to a reduced screening accompanied with an increase of the ionic repulsion. This may explain why for the capped triangular bipyramid and the pentagonal pyramid clusters, the interatomic distances are not reduced as compared with their neutral counterparts despite having lower spin magnetic moments.

We have found several spin states for each one of the isomers quoted in Table 1, all having $\leq$10 meV excess energy per atom and nearly zero HOMO−LUMO gap. For example, the prism isomer of Rh_6^+ has two spin isomers with total magnetic moment 5 and 7 μ_B at 1.0 and 4 meV excess energy per atom, respectively, both with zero HOMO−LUMO gap. Similarly, for the octahedral isomer of Rh_6^+ we obtained two spin isomers with total magnetic moment 7 and 5 μ_B, at 9 and 67 meV excess energy per atom, respectively, both with nearly zero HOMO−LUMO gap. However, for the ground state spin state of the octahedron and prism isomers, given in Table 1, we obtained HOMO−LUMO gaps of 0.11 and 0.17 eV, respectively.

As regards the anionic Rh_6^- cluster, we note first that the ground state is now the triangular prism instead of the octahedron (the two most stable structures found for the neutral and positively charged clusters, reverse their energetic order here). Moreover, the total energy differences among the isomers are reduced as compared with the neutral case (the opposite happened for the cationic cluster), and the increase of an electron is also accompanied by a change of the spin state, though not always in the same direction. The several spin states of the octahedral Rh_6^- cluster, including the lowest energy one, have all nearly zero HOMO−LUMO gap. Instead, the lowest energy spin state of the prism isomer, that is, the ground state, has a 0.14 eV HOMO−LUMO gap. The geometrical structures of the neutral clusters shown in Figure 1 are essentially preserved. Therefore, as a general trend from the energetic point of view, we find that the total energy differences increase with decreasing charge density, i.e., in going from Rh_6^- to Rh_6 and to Rh_6^+, which correlates with the increase of the electron screening. This trend indicates that the octahedron isomer becomes more stable with respect to higher order isomers when the charge density decreases, which may happen upon adsorption of certain light molecules with electronegativity higher than the rhodium cluster.

The next subsection is devoted to the detailed analysis of the NO adsorption on the ground state and on the first isomer of Rh_6^+.

B. Adsorption of NO on the Octahedron and Prism-Type Isomers of Rh_6^+. It is pertinent to perform a systematic study of the adsorption of NO on both the ground state (octahedron) and the first isomer (prism) of the bare cluster Rh_6^+. These isomers could coexist, in view of the results discussed in the previous subsection. NO adsorption can be realized in different ways, dissociative or molecularly, and on different sites of the cluster, i.e., on top, bridge, or hollow configurations. Therefore, there are plenty of possibilities and we have endeavored to test all of them by taking as input a large variety of atomic arrangements for the adsorption process, as well as different spin states. We have calculated the relevant energies (total energy differences and adsorption energies) in all cases. The NO adsorption energy for a given configuration Rh_6^+−NO is calculated as follows:

$$E_{ad} = E(Rh_6^+) + E(NO) - E(Rh_6^+\text{−NO})$$

where the final configuration Rh_6^+−NO and the initial isolated Rh_6^+ and NO clusters are conveniently structurally relaxed.

In Figure 2 we illustrate the results for the NO adsorption on the ground state octahedron cluster Rh_6^+. Figure 3 shows the results for the adsorption on the first isomer with prism-type structure. We discuss first the results in Figure 2. From the difference in total energy, the most stable Rh_6^+−NO configuration corresponds to the dissociative adsorption of NO, with the N adsorbed in a hollow site and the O in a bridge configuration, with a N−O interatomic distance of 3.16 Å and a total magnetic moment of 4 μ_B. That configuration is denoted bridge−hollow I in Figure 2. In the configuration hollow−hollow I of Figure 2, with a total energy difference of 53 meV, both N and O are adsorbed on hollow sites with an N−O interatomic distance of 3.49 Å. In both configurations N and O are connected by a Rh atom forming angles ∠NRhO of 110° (bridge−hollow) and 130° (hollow−hollow), respectively. The adsorption of NO is accompanied by a decrease of the magnetic moment of the Rh_6^+ host. In the hollow−hollow configuration II of Figure 2, with 230 meV higher energy, the N and O atoms are not connected by any single Rh atom, whereas in the hollow−hollow III state they are connected by two Rh atoms. The hollow−hollow (h−h) configurations show higher Rh−O distances and higher magnetic moments than the bridge−hollow (b−h) I isomer.

The nearly degenerate bridge−hollow I and hollow−hollow I isomers differ mainly in the O atom adsorption site, which is

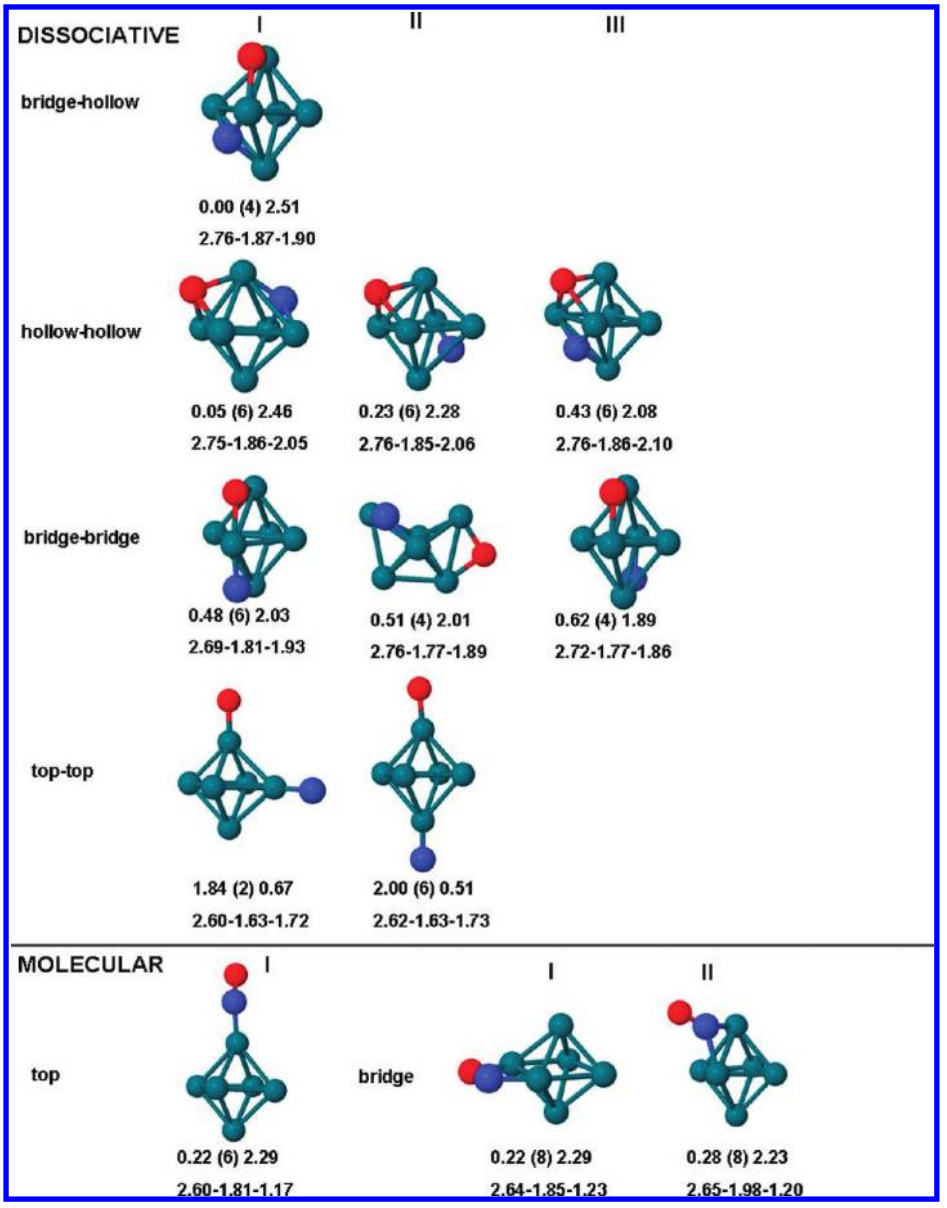

Figure 2. Several configurations of the Rh_6^+−NO complex resulting from dissociative (upper panel) and molecular (lower panel) adsorption of NO on the O_h isomer of Rh_6^+ cation (ground state). Red, blue, and green balls correspond to oxygen, nitrogen, and rhodium, respectively. For each configuration, two sets of data are given: in the first row are quoted the total energy (eV) relative to that of the lowest energy configuration, the total magnetic moment (μ_B) in parentheses, and the adsorption energy (eV) as defined in the text, respectively; in the second row are given the Rh−Rh (average), Rh−N, and Rh−O (N−O for the molecularly adsorption configurations) distances (Å), respectively. Notice that the sum of the total relative energy and the adsorption energy is the binding energy of the strongest bonded complex (2.51 eV).

extremely sensitive to the charge environment (see, for example, the case of $Rh_6(CO)_m^+$ complexes for transitions from bridge to atop positions of the carbonyl[42]). That can be illustrated by examining the magnetic moment and corresponding HOMO−LUMO gap values for the different configurations. Thus, the bridge−hollow I configuration of Figure 2 with 4 μ_B (6 μ_B) total magnetic moment has 0.34 (0.04) eV HOMO−LUMO gap, and the hollow−hollow I configuration of Figure 2 with 6 μ_B (4 μ_B) total magnetic moment has 0.31 (0.31) eV HOMO−LUMO gap. The relatively high HOMO−LUMO values of b−h I (with 4 μ_B) and h−h I (with 6 μ_B and 4 μ_B) structures suggest that the octahedral based complexes are structurally stable against a small amount of charge variations.

At higher energies (between 219 and 282 meV) we find, together with the dissociative hollow−hollow II configuration, three Rh_6^+−NO clusters with molecularly adsorbed NO, in all cases with the molecule bound through the N atom, and preferably in an atop configuration (the less stable of these clusters corresponds to adsorption in a bridge configuration, configuration II in the lower panel of Figure 2). The molecular adsorption implies short interatomic N−O distances in the range 1.2 Å. The experimental (calculated) bond distance in the free molecule is 1.15 (1.17) Å. At even higher energy difference, other Rh_6^+−NO clusters appear with a variety of dissociative adsorption of NO in different positions over the rhodium cluster, preferentially in high coordinated sites (bridge and/or hollow).

dx.doi.org/10.1021/jp202511w |J. Phys. Chem. A 2011, 115, 8350–8360

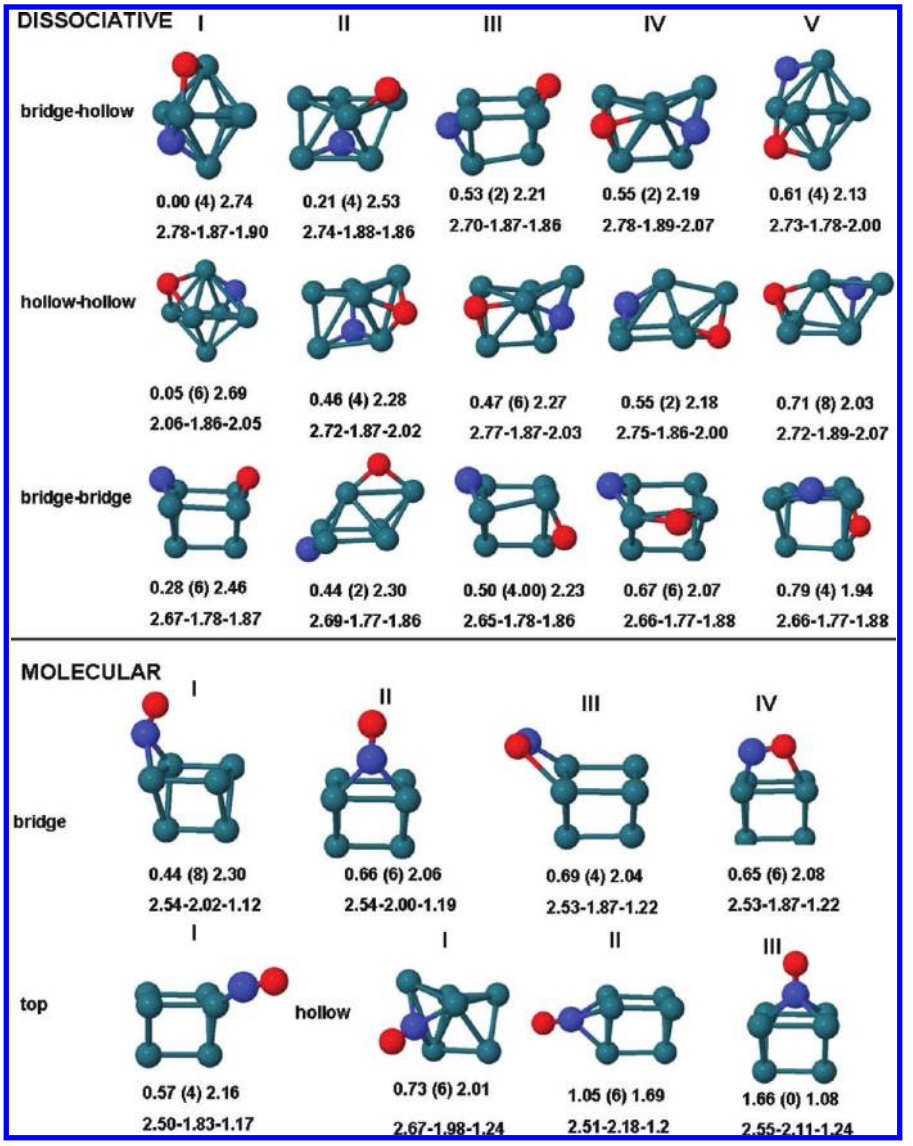

Figure 3. Several configurations of Rh_6^+—NO complex resulting from dissociative (upper panel) and molecular (lower panel) adsorption of NO on the prism isomer of Rh_6^+ cation. The two sets of data below each configuration have the same meaning as in Figure 2, the adsorption energies being calculated now with respect to the prism isomer of Rh_6^+.

The two dissociative configurations (the top-top configurations in Figure 2) with N and O on top of different Rh atoms are less favored energetically. We note that in all cases, the octahedral symmetry of the Rh_6^+ cluster is preserved to a great extent upon NO adsorption, which reflects the stability of this structure, being the ground state of both the neutral and positively charged six-atoms rhodium cluster. Similar high stability upon removal of an electron has been reported for neutral $Rh_6(CO)_m$ complexes with T_d symmetry having an octahedral Rh_6 metal core.[42] Only the dissociative bridge—bridge adsorption (configuration II in Figure 2) departs from the O_h symmetry of the Rh_6^+ ground state and looks like the third isomer of Rh_6^+ in Figure 1. Notice that for both II and III bridge—bridge isomers the N and O atoms are adsorbed on edges without common Rh atoms. The magnetic moment of these b—b isomers is smaller than that of the b—b I isomer.

As regards the NO adsorption on the triangular prism isomer of Rh_6^+, remarkable structural deformations are found in many cases and, therefore, we have calculated more configurations (Figure 3). Here, the adsorption is accompanied by a strong distortion of the prism symmetry of Rh_6^+, particularly when the dissociated NO is adsorbed in high coordinated sites. As was found for the ground state octahedral Rh_6^+, dissociative adsorption is the most favorable process. And what is more interesting, in the most stable configuration of Rh_6^+—NO, the triangular prism is dramatically deformed to finally reach a geometry that exactly matches the most stable arrangement found for NO adsorbed on the ground state octahedron Rh_6^+, that is, a dissociative adsorption with N in hollow and O in bridge sites (note that exchange of N and O adsorption sites leads to an equilibrium configuration that is 0.61 eV less stable: N prefers coordination 3 and O prefers coordination 2; see configuration bridge—hollow V in Figure 3). In other words, the triangular prism evolves to an octahedron upon NO adsorption. Not only this, but also the second most stable arrangement (configuration I of hollow—hollow in Figure 3) corresponds to the second most

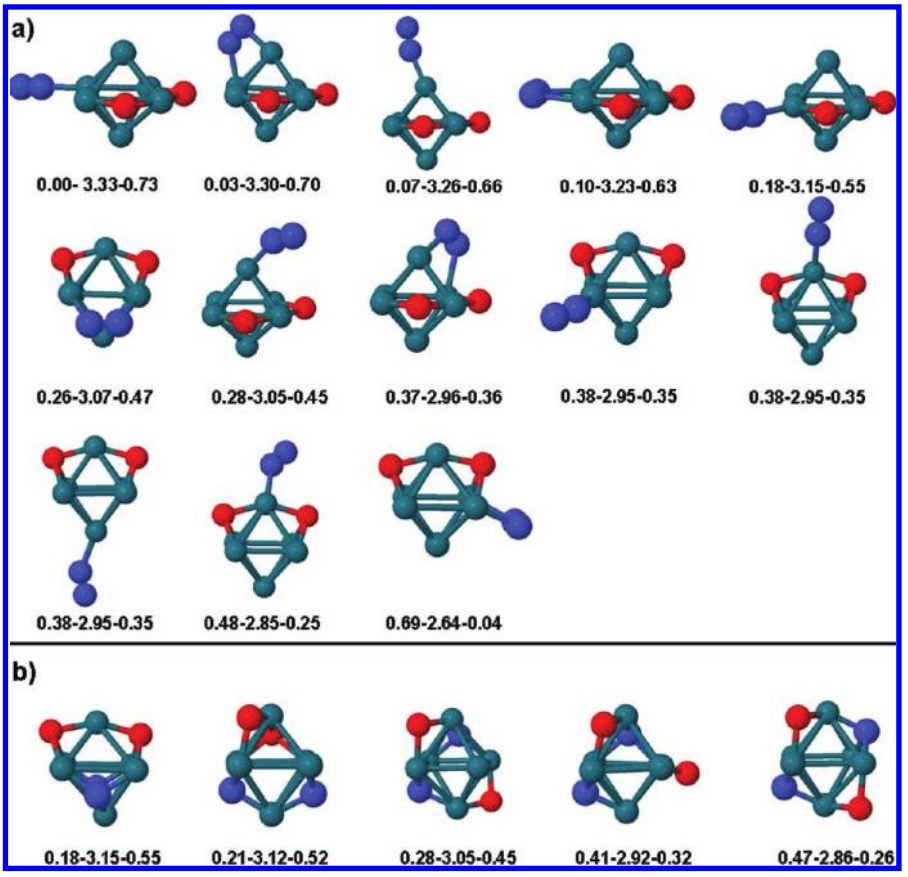

Figure 4. (a) Several optimized configurations of $Rh_6O_2^+-N_2$ complexes with a preformed N_2 molecule and dissociated O_2. The total energy with respect to the lowest energy conformer is given below (eV). The magnetic moment is the same ($5\,\mu_B$) for each configuration. The formation energy (Δ) of these intermediate complexes with respect to the ground state of the separated Rh_6^+-NO complex and NO molecule, together with the desorption energy (δ) of N_2 from $Rh_6^+-(NO)_2$ intermediate complexes with respect to the ground state of the separated $Rh_6^+-O_2$ complex and N_2 molecule are also given. (b) Configurations of $Rh_6^+-(NO)_2$ complexes with dissociated N_2 and O_2. The data are as in the upper panel, and the magnetic moment is $1\,\mu_B$ for each configuration.

stable arrangement found for the octahedron Rh_6^+. The analysis of the electronic population shows that upon NO adsorption the substrate loses 0.6 e^- in favor of N (it gains 0.23 e^-) and O (it gains 0.37 e^-), as compared with the bare Rh_6^+. As indicated in the previous section, a decrease of the charge density tends to stabilize the octahedron with respect to other isomers, in particular the triangular prism.

This result deserves a deeper discussion in connection with the experiments, in the next section. Different degrees of distortion of the prism take place for the various dissociatively adsorbed NO configurations next in stability, although one can distinguish the third isomer of Rh_6^+ in Figure 1 as part of the II and IV bridge−hollow configurations as well as II and III hollow−hollow configurations. One can recognize also the variety of magnetic moment in a narrow range of energy of the hollow−hollow and bridge−bridge configurations. Magnetic isomers of the b−b I configuration with 4, 5, and 6 μ_B were found having energy difference smaller than 27 meV.

In contrast, molecular adsorption of NO leads, in general, to a slight or negligible distortion of the prism (exception is the hollow I configuration); molecular adsorption is preferably done on atop or bridge sites with the molecule always bound through the N atom (Figure 3).

C. Adsorption of NO on Low Energy Rh_6^+-NO Complexes. Starting with the bridge−hollow I and hollow−hollow I and II dissociative configurations, as well as the molecularly adsorbed top I and bridge I configurations of Rh_6^+-NO complexes shown in Figure 2, we have considered the adsorption of a second NO molecule in many different sites as initial $Rh_6^+-(NO)_2$ structures. After relaxation of a big set of such trial structures, we have realized that those configurations containing a preformed N_2 molecule, denoted as $Rh_6O_2^+-N_2$, have smaller total energy than other equilibrium conformations, and that those $Rh_6O_2^+-N_2$ complexes showing dissociated O_2 have even lower energy than the others. A selection of several configurations of that type is shown in Figure 4, together with the total energy, relative to the lowest one. The magnetic moment of all these conformers is $5\,\mu_B$. Two other magnitudes are also given for each conformer, namely, the binding energy of the second NO (Δ), and the N_2 desorption energy (δ). The largest desorption energy of the N_2 molecule is $\delta = 0.7$ eV. These energies are defined as

$$\Delta = E(Rh_6^+-NO) + E(NO) - E(Rh_6O_2^+-N_2)$$

and

$$\delta = E(Rh_6^+-O_2) + E(N_2) - E(Rh_6O_2^+-N_2)$$

respectively. In these expressions $E(Rh_6O_2^+-N_2)$ is the energy of a given complex with a preformed N_2 molecule, and $E(Rh_6^+-NO)$ ($E(Rh_6^+-O_2)$) represents the lowest energy of the more stable

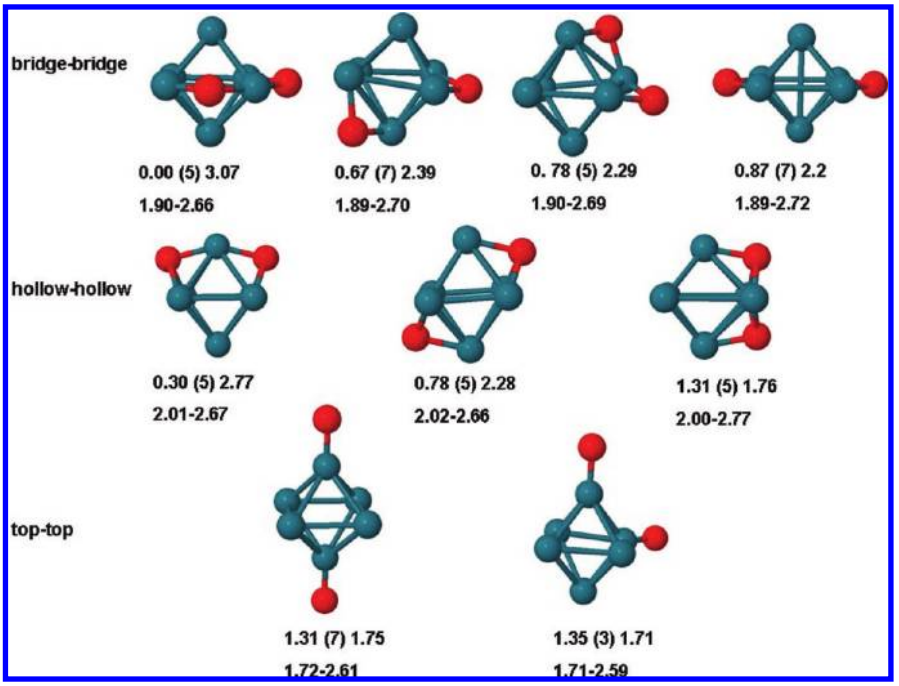

Figure 5. Several optimized configurations $Rh_6^+-O_2$ complexes with dissociated O_2. For each configuration, two sets of data are given: in the first row are quoted, respectively, the total energy (eV) relative to that of the lowest energy configuration, the total magnetic moment (μ_B) in parentheses, and the O_2 dissociative adsorption energy (eV) defined as $E(Rh_6^+) + E(O_2) - E(Rh_6^+-O_2)$; in the second row are given the average O−Rh and Rh−Rh distances (Å), respectively.

Rh_6^+-NO ($Rh_6^+-O_2$) complex, respectively. Similarly, $E(NO)$ and $E(N_2)$ represent the ground state energy of NO and N_2 molecules, respectively.

The quantity $\Delta - \delta$ is the variation of energy between the intermediates of the step reaction

$$Rh_6^+-NO + NO \rightarrow Rh_6^+-O_2 + N_2$$

and has the constant value 2.6 eV. The value of 2.6 eV becomes reduced (enhanced) when the step reaction occurs between higher energy $Rh_6^+-O_2$ (Rh_6^+-NO) isomers.

We have also obtained $Rh_6O_2^+-N_2$ complexes with two separated N and O atoms bonded on different sites of the b−h I or h−h I Rh_6^+-NO configurations in Figure 2. Some isomers of that type are represented in the lowest panel of Figure 4. The more tightly bound of these complexes has 0.18 eV total energy excess with respect to the ground state in Figure 4, and the N and O atoms are bonded, respectively, on symmetrical positions of the N and O atoms of the h−h I isomer of Figure 2. The complex with 0.21 eV energy is similarly obtained starting with the b−h I isomer of Figure 2.

In this paper we study the successive adsorption of two NO molecules on Rh_6^+. This corresponds to the first reaction steps of the whole mechanism proposed by Ford et al.[4] for understanding the catalytic process when further NO molecules are adsorbed until the species Rh_6^+ becomes saturated with oxygen and thus catalytically "poisoned".

In Figure 5 are shown several low lying energy configurations of $Rh_6^+-O_2$ complexes formed by dissociative adsorption of an O_2 molecule on the Rh_6^+ cation. The equilibrium configurations with molecularly adsorbed O_2 have much smaller binding energy and are not shown. The lowest energy complex in Figure 5, with two separated O atoms occupying adjacent 2-fold bridging positions, is assumed to be the product of the reaction sketched above. Notice that the Rh_6^+ substrate cluster is nearly undistorted compared to the rectangular bipyramid ground state of the bare cluster. These features are similar to those found experimentally for the adsorption geometry of two O atoms on $TM4_6^+$ clusters (TM4 = V, Nb, Ta),[43] whose ground state geometry is also a rectangular bipyramid. These TM4 atoms have a s^2d^3 configuration with 3d electrons, which is complementary to the s^2d^7 configuration of Rh. For each configuration in Figure 5 is given its total energy relative to the lowest energy one, the magnetic moment (in parentheses), and the adsorption energy of O_2. The average Rh−Rh and Rh−O bond lengths (in Å), respectively, are also given in the second line of data. On the other hand, the two lower-total energy isomers of $Rh_6^+-O_2$ (the first ones of the two first rows) are similar to the two first early degenerate structures obtained by Harding et al.,[6] although these authors optimized them only in the octect spin to roughly map out the low-energy geometries from which to build the trioxide input structures. The energy difference so obtained by these authors was only 0.09 eV whereas we have obtained a difference of 0.30 eV, being the bridge sites (and not high-coordination ones) clearly preferred by the two oxygen atoms.

Similar data are given for the $Rh_6^+-N_2$ complexes shown in Figure 6. For these complexes, in contrast to $Rh_6^+-O_2$ ones, the preferred complexes are molecularly adsorbed, resulting in the atop and bridge adsorption configurations with the same binding energy ~0.71 eV. Dissociative adsorption of N_2 on Rh_6^+ appears at excitation energies of $Rh_6^+-N_2$ complexes larger than 0.16 eV, and for ~1.04 eV excitation energy the N atoms are no longer supported on the Rh_6^+ cluster.

IV. DISCUSSION

For small clusters, the effect of an extra electron or hole does not get strongly diluted over the cluster and the change in the electron density can influence the adsorption behavior of light

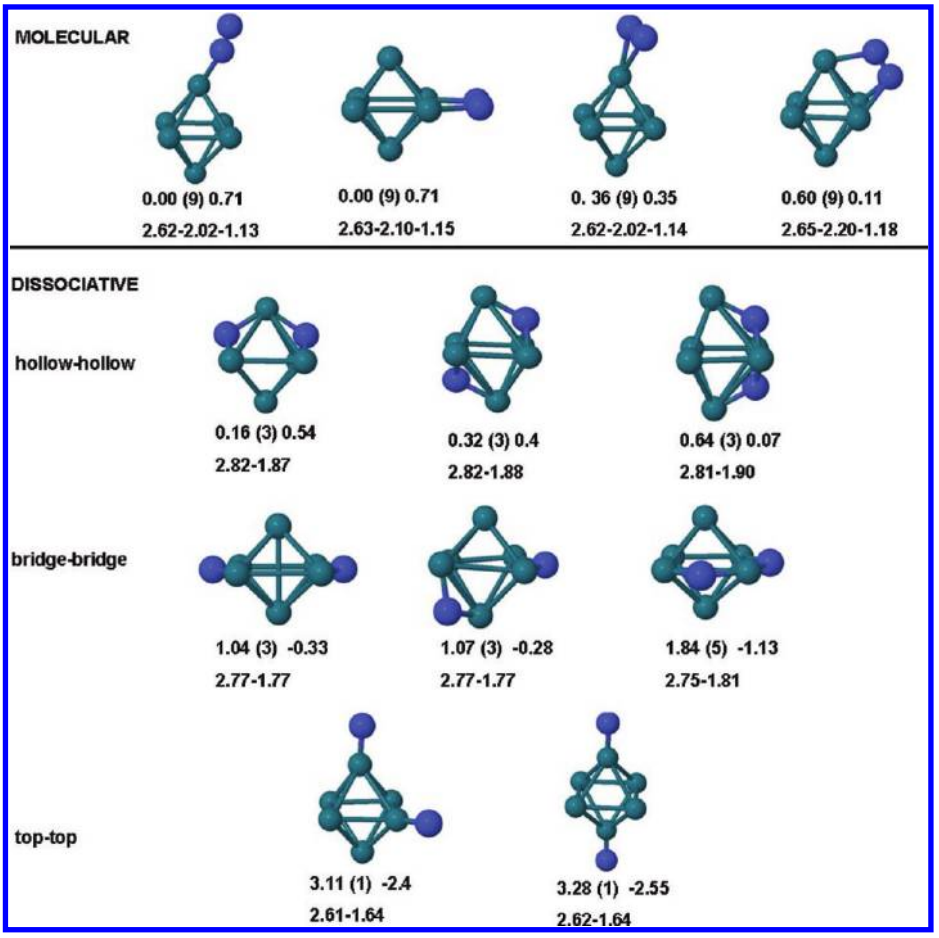

Figure 6. Several optimized configurations of $Rh_6^+-N_2$ complexes. For each configuration, two sets of data are given: in the first row are quoted, respectively, the total energy (eV) relative to that of the lowest energy configuration, the total magnetic moment (μ_B) in parentheses, and the N_2 adsorption energy (eV) defined as $E(Rh_6^+) + E(N_2) - E(Rh_6^+-N_2)$; in the second row are given the average Rh−Rh and Rh−N distances (Å), respectively.

molecules.[44] For example, in the case of CO adsorption for the higher coordination sites, clear charge state dependence is observed.[42] The CO binds in hollow sites for the neutral and cationic tetramer, while for the anion only atop binding is observed.[45] With decreasing electron density, the tendency to high coordination adsorption like in the hollow (or face capping) configuration increases. This tendency has been experimentally observed through infrared multiple photon dissociation (IR-MPD) spectroscopy for clusters of the 4d elements Ru, Rh, and Pd and some of the 5d[45] and our results support this experimental finding in the case of NO adsorption.

As regards the adsorption of NO on the cluster Rh_6^+, the experimental results of Ford and co-workers through FT-ICR mass spectrometry,[4] have shown a marked biexponential decay of the bare Rh_6^+ ion intensity upon reaction with NO, which is interpreted as the presence of two isomeric forms in the original Rh_6^+ population. Our results support the coexistence of the ground state and the first isomer with octahedral and prism-type structures, respectively. The ground state octahedral structure and the isomer with prism-type structure could give rise to the markedly different NO adsorption rates experimentally observed, as suggested by Ford et al.[4] The initial population of Rh_6^+ is expected to contain more isomers of octahedral symmetry, provided the higher stability of this cluster than of the prism one. Besides, the energy of NO adsorption on the octahedron is clearly larger than that on the prism isomer. Therefore, the presence of both isomers, together with their significantly different adsorption energies, can explain the experimentally observed biexponential decay.

Ford et al.[4] have found that good fits of the kinetic data obtained when further NO is adsorbed on the rhodium cluster are obtained by assuming that those two different isomeric forms are only relevant in the first step, that is, for the adsorption of the first NO. Our results can explain this scenario as a consequence of the structural transition undergone by the triangular prism isomer upon NO adsorption, leading to the same arrangement found for NO adsorbed on the ground state octahedron Rh_6^+ isomer. This means that after the initial step of NO adsorption, only octahedral isomers should be present in the sample, that is, a single isomeric form. Moreover, to be consistent with the appearance of particular peaks in the mass spectra and the absence of others, Ford and co-workers concluded that the adsorption of the first NO has to be dissociative and, on the basis of the observations of NO adsorption on the Rh(111) surface,[9,10,15] the authors propose a reaction mechanism based on the NO adsorption taking place preferentially in 3-fold binding sites of the octahedral Rh_6^+. Our results and the analysis based on the stability of the final products, confirm the

dissociative adsorption. We obtain dissociative adsorption as the most stable process in both the octahedron and the prism Rh_6^+ clusters, as indicated in the previous section. However, our most stable configuration corresponds to a bridge−hollow adsorption process instead of the hollow−hollow one which would fit the adsorption on the 3-fold binding sites. This is 50 meV less stable, although its adsorption energy is only 5 meV lower than the bridge−hollow's one. It is important to note that although 3-fold sites exist in both the (111) fcc surface and the O_h symmetry of the octahedral Rh_6^+, the local environments are different and, consequently, also the electronic structures. Besides, quantum confinement effects typical of the small finite size regime are not present at extended surfaces.

Recent improved IR-MPD experiments combined with DFT calculations[21] have suggested that N_2O molecule bonds atop of Rh_6^+ through the extreme N atom and that configuration evolves via several intermediate states to a $Rh_6O^+-N_2$ complex from which N_2 can be desorbed to yield Rh_6O^+ cluster. A similar study[21] for the $Rh_6O(N_2O)^+$ complex provided some evidence of the formation of $Rh_6^+-O_2$, implying surface reactions in $Rh_6O(N_2O)^+$, but experiments are not resolved enough to affirm that unambiguously.[21]

From our calculations for the adsorption of NO on Rh_6^+-NO complexes, we see that the $Rh_6O_2^+-N_2$ complexes in the first row of Figure 4 have a $Rh_6^+-O_2$ substrate with the same geometry as the lowest energy $Rh_6^+-O_2$ cluster (Figure 5), and all of them are within a narrow energy interval <0.2 eV. Moreover, the N_2 preformed molecule of all $Rh_6O_2^+-N_2$ complexes is similar to that of the two first Rh_6-N_2 isomers. In particular, the three first conformers in Figure 4 are practically degenerate, which point to a high mobility of the preformed N_2. These facts are in qualitative agreement with the experiment.[4]

The second and third $Rh_6O_2^+-N_2$ complexes in the second row of Figure 4 differ from the third and second complexes in the first row, respectively, in the different orientation of the preformed N_2 with respect to the two O atoms of the $Rh_6^+-O_2$ substrate, suggesting that the N_2 molecule avoids the proximity of oxygen atoms. The remaining conformers of $Rh_6O_2^+-N_2$ complexes in Figure 4 have a $Rh_6^+-O_2$ substrate with the same geometry as the first hollow−hollow isomer of $Rh_6^+-O_2$ (Figure 5). Three of these complexes (the fourth and fifth ones of the second row and the first one in the third row) are degenerate, illustrating again the easy mobility of N_2 between available Rh_6^+ atop positions.

V. SUMMARY

Using the density-functional theory as implemented in the SIESTA code, with the generalized gradient approximation, we have studied the consecutive adsorption of two NO molecules on the cationic cluster Rh_6^+. Our results for the bare Rh_6^+ support the coexistence of the ground state octahedral cluster and the first isomer with prism-type structure. Therefore, the presence of both isomers, together with their significantly different adsorption energies, can explain the biexponential decay due to the markedly different NO adsorption rates experimentally observed through Fourier transform ion cyclotron resonance (FT-ICR) mass spectrometry by Ford et al.[4]

Our results confirm the dissociative adsorption of NO, in agreement with the experimental interpretation of the data. We obtain dissociative adsorption as the most stable configuration in both the octahedron and the prism Rh_6^+ clusters. The most stable Rh_6^+-NO configuration corresponds to the dissociative adsorption of NO, with the N adsorbed in a hollow site and the O in a bridge configuration. In the next more stable configuration, both N and O are adsorbed on hollow sites.

The structural transition undergone by the triangular prism isomer upon NO adsorption, leading to the same arrangement found for on the ground state octahedron Rh_6^+ isomer, indicates that after the initial reaction step of NO adsorption, only octahedral isomers should be present in the sample, that is, a single isomeric form. This trend is consistent with Ford et al.'s kinetic data, for which a good fit is obtained by the experimental group assuming that the two different isomeric forms are only relevant in the first step of the process, that is, for the adsorption of the first NO.

On the other hand and with respect to the second NO adsorption on Rh_6^+-NO, the calculated $Rh_6-(NO)_2$ complexes have a Rh_6O_2 substrate with the same geometry as the lowest energy $Rh_6O_2^+$ cluster and a preformed N_2 molecule that avoids the proximity of oxygen atoms. The different degenerate structures point to a high mobility of the preformed N_2. The N_2 desorption energy is about 0.7 eV to give the $Rh_6^+-O_2$ complex with two separated O atoms occupying adjacent 2-fold bridging positions of the nearly undistorted Rh_6^+ octahedral cluster. These facts are in qualitative agreement with the experiment.

The next step in our study will be to investigate the adsorption of further NO molecules, taking as the starting points the most stable configurations found here for Rh_6^+-NO and $Rh_6^+-(NO)_2$ complexes. These calculations represent a substantial undertaking. Work in this line is under progress.

AUTHOR INFORMATION

Corresponding Author
*E-mail: begonia@ubu.es.

ACKNOWLEDGMENT

M.B.T. acknowledges the advice and expertise offered by A. Muñoz from the University of Burgos and M. A. Rodriguez from the University of La Rioja. We acknowledge the financial support from the Spanish Ministry of Science and Innovation (Project FIS2008-02490) in conjunction with the European Regional Development Fund and by the Junta de Castilla y León (Project No. GR120). F.A-G. acknowledges the financial support from PROMEP-SEP-CA230 and computer resources from the Centro Nacional de Supercomputo (CNS) from the IPICyT, San Luis Potosí, S.L.P., México

REFERENCES

(1) Cox, A. J.; Louderback, J. G.; Apsel, S. E.; Bloomfield, L. A. *Phys. Rev. B* **1994**, *49*, 12295.
(2) Beyer, M. K.; Knickelbein, M. B. *J. Chem. Phys.* **2007**, *126*, 104301.
(3) Balteanu, I.; Achatz, U.; Balajl, O. P.; Fox, B. S.; Beyer, M.; Bondybey, V. E. *Int. J. Mass Spectrom.* **2003**, *229*, 61.
(4) Ford, M. S.; Anderson, M. L.; Barrow, M. P.; Woodruff, D. P.; Drewello, T.; Derrick, P. J.; Mackenzie, S. R. *Phys. Chem. Chem. Phys.* **2005**, *7*, 975.
(5) Anderson, M. L.; Ford, M. S.; Derrik, P. J.; Drewello, T.; Woodruff, D. P.; Mackenzie, S. R. *J. Phys. Chem. A* **2006**, *110*, 10992.
(6) Harding, D.; Mackenzie, S. R.; Walsh, T. R. *J. Phys. Chem. B* **2006**, *110*, 18272.

(7) Harding, D.; Ford, M. S.; Walsh, T. R.; Mackenzie, S. R. *Phys. Chem. Chem. Phys.* **2007**, *9*, 2130.
(8) Harding, D.; Davies, D. L.; Mackenzie, S. R.; Walsh, T. R. *J. Chem. Phys.* **2008**, *129*, 124304.
(9) Brown, W. A.; King, D. A. *J. Phys. Chem. B* **2000**, *104*, 2578.
(10) Johánek, V.; Schauermann, S.; Laurin, M.; Gopinath, C. S.; Libuda, J.; Freund, H. F. *J. Phys. Chem. B* **2004**, *108*, 14244.
(11) Zhdanov, V. P.; Kasemo, B. *Surf. Sci. Rep.* **1997**, *29*, 31.
(12) Loffreda, D.; Delbecq, F.; Simon, D.; Sautet, J. *J. Chem. Phys.* **2001**, *115*, 8101.
(13) Mavrikakis, M.; Rempel, J.; Greeley, J.; Hansen, L. B.; Nørskow, J. K. *J. Chem. Phys.* **2002**, *117*, 6737.
(14) Belton, D. N.; Dimaggio, C. L.; Schmieg, S. J.; Ng, K. Y. S. *J. Catal.* **1995**, *157*, 559.
(15) Jinlong, Y.; Toigo, F.; Kelin, W. *Phys. Rev. B* **1994**, *50*, 7915.
(16) Ghosh, P.; Pushpa, R.; de Gironcoli, S.; Narasimhan, S. *Phys. Rev. B* **2009**, *80*, 233406.
(17) Rempel, J.; Greeley, J.; Hansen, L. B.; Nielsen, O. H.; Nørskov, J. K.; Mavrikakis, M. *J. Phys. Chem. C* **2009**, *113*, 20623.
(18) Parks, E. K.; Nieman, G. C.; Kerns, K. P.; Riely, S. J. *J. Chem. Phys.* **1997**, *107*, 1861.
(19) Xing, X.; Yoon, B.; Landman, U.; Parks, J. H. *Phys. Rev. B* **2006**, *74*, 165423.
(20) Gruene, P.; Rayner, D. M.; Redlich, B.; van der Meer, A. F. G.; Lyon, J. T.; Meijer, G.; Fielicke, A. *Science* **2008**, *321*, 674.
(21) Hamilton, S. M.; Scott Hopkins, W.; Harding, D. J.; Walsh, T. R.; Gruene, P.; Haertelt, M.; Fielicke, A.; Meijer, G.; Mackenzie, S. R. *J. Am. Chem. Soc.* **2010**, *132*, 1448.
(22) Hamilton, S. M.; Scott Hopkins, W.; Harding, D. J.; Walsh, T. R.; Haertelt, M.; Kerpal, C.; Gruene, P.; Meijer, G.; Fielicke, A.; Mackenzie, S. R. *J. Phys. Chem. A* **2011**, *115*, 2489.
(23) Yudanov, I. V.; Shnoum, R.; Neymn, K. M.; Rösch, N. *J. Chem. Phys.* **2002**, *117*, 9887.
(24) Reddy, B. V.; Nayak, S. K.; Khanna, S. N.; Rao, B. K.; Jena, P. *Phys. Rev. B* **1999**, *59*, 5214.
(25) Bae, Y. C.; Kumar, V.; Osanai, H.; Kawazoe, Y. *Phys. Rev. B* **2005**, *72*, 125427.
(26) Futschek, T.; Marsman, M.; Hafner, J. *J. Phys. Condens. Matter* **2005**, *17*, 5927.
(27) Aguilera-Granja, F.; Balbás, L. C.; Vega, A. *J. Phys. Chem. A* **2009**, *113*, 13483.
(28) Soler., J. M.; Artacho, E.; Gale, J. D.; Garca, A.; Junquera, J.; Ordejon, P.; Sánchez-Portal, D. *J. Phys.: Condens. Matter* **2002**, *14*, 2745.
(29) Troullier, N.; Martins, J. L. *Phys. Rev. B* **1991**, *43*, 1993.
(30) Troullier, N.; Martins, J. L. *Phys. Rev. Lett.* **1982**, *48*, 1425.
(31) Perdew, J. P.; Burke, K.; Ernzerhof, M. *Phys. Rev. Lett.* **1996**, *77*, 3865.
(32) Louie, S. G.; Froyen, S.; Cohen, M. L. *Phys. Rev. B* **1982**, *26* (4), 1738.
(33) Boys, S. F.; Bernardy, F. *Mol. Phys.* **1970**, *19*, 553.
(34) The experimental values are taken from refs 31, 35, and 36.
(35) Zhang, Y.; Yang, W. *Phys. Rev. Lett.* **1998**, *80*, 890.
(36) Hammer, B.; Hansen, L. B.; Nørskov, J. K. *Phys. Rev. B* **1999**, *71*, 165421.
(37) Dion, M.; Rydberg, H.; Schröder, E.; Langreth, D. C.; Lundqvist, B. I. *Phys. Rev. Lett.* **2004**, *92*, 246401.
(38) Román-Pérez, G.; Soler, J. M. *Phys. Rev. Lett.* **2009**, *103*, 096102.
(39) Odashima, M. M.; Capelle, K. J. M. *Phys. Rev. A* **2009**, *79*, 062515.
(40) Harding, D. J.; Walsh, T. R.; Hamilton, S. M.; Hopkins; Mackenzie, S. R.; Gruene, P.; Haertelt, M.; Meijer, G.; Fielicke, A. *J. Chem. Phys.* **2010**, *132*, 011101.
(41) Harding, D. J.; Gruene, P.; Haertelt, M.; Meijer, G.; Fielicke, A.; Hamilton, S. M.; Hopkins, W. S.; Mackenzie, S. R.; Neville, S. P.; Walsh, T. R. *J. Chem. Phys.* **2010**, *133*, 214304.
(42) Swart, I.; de Groot., F. M. F.; Weckhuysen, B.; Rayner, D. M.; Meijer, G.; Fielicke, A. *J. Am. Chem. Soc.* **2008**, *130*, 2126.
(43) Fielicke, A.; Gruene, P.; Haertelt, M.; Harding, D. J.; Meijer, G. *J. Phys. Chem. A* **2010**, *114*, 9755.
(44) Swart, I.; de Groot., F. M. F.; Weckhuysen, B.; Rayner, D. M.; Meijer, G.; Fielicke, A. *J. Chem. Phys.* **2006**, *124*, 194305.
(45) Fielicke, A.; Gruene, P.; Meijer, G.; Rayne, D. M. *Surf. Sci.* **2009**, *603*, 1427.